Field line resonances in a stretched magnetotail: CANOPUS optical and magnetometer observations

J. A. Wanliss, R. Rankin, and J. C. Samson

Department of Physics, University of Alberta, Edmonton, Alberta, Canada

V. T. Tikhonchuk[1]

P. N. Lebedev Physics Institute, Russian Academy of Science, Moscow, Russia

[1] Ground-based observations support the existence of $1-4$ mHz field line resonances (FLRs) at auroral latitudes. The low frequencies suggest that many nightside FLRs are excited on stretched magnetic field lines in the inner plasma sheet. Data from the Canadian Auroral Network for the OPEN Program Unified Study (CANOPUS) magnetometers and photometers on 21 February 1993 indicate a FLR with a peak at 2.4 mHz, and that of 31 January 1997 indicate a peak at 1.3 mHz. In this paper, models of FLRs and models of stretched magnetotail topologies deduced from optical data are compared with the observations. The FLR model is independently constrained by a parametric near-Earth magnetotail model that allows us to make direct comparisons with the observed FLR frequency. For the two case studies mentioned above, we are able to show that the theoretical FLR spectrum, computed on stretched field lines, is comparable to the low-frequency experimental observations. *INDEX TERMS:* 2407 Ionosphere: Auroral ionosphere (2704); 2447 Ionosphere: Modeling and forecasting; 2788 Magnetospheric Physics: Storms and substorms; *KEYWORDS:* Auroral mapping, field line resonances, topology

1. Introduction

[2] Low-frequency shear Alfvén field line resonances (FLRs) are often observed within H_β (486.1 nm) optical emissions on magnetic field lines threading the equatorward edge of the auroral zone. FLRs have wave fields, field-aligned currents, and plasma flow topologies that are remarkably similar to those found in a class of discrete auroral arcs that is associated with narrowband shear Alfvén waves (SAWs) [*Samson et al.*, 1996; *Tröndsen et al.*, 1997]. FLRs have been observed in the context of numerous spacecraft and ground-based observations [*Ruohoniemi et al.*, 1991; *Lotko et al.*, 1998] and studied extensively using numerical models [*Streltsov and Lotko*, 1999; *Rankin et al.*, 1999, 2000]. Coupling of global-scale compressional waves to standing SAWs can explain energy accumulation on resonant field lines where the frequency of the compressional waves matches the local field line eigenfrequency. Near the ionosphere the large currents (up to ~ 10 μA m^{-2}) associated with the FLRs can potentially explain parallel electric fields in the auroral accelerator.

[3] FLRs on field lines threading the auroral ionosphere have been seen in HF radar observations [*Ruohoniemi et al.*, 1991; *Fenrich et al.*, 1995] and in ground-based magnetometer [*Samson et al.*, 1996] and optical observations [*Samson et al.*, 1991, 1996]. They typically have frequencies in the range of $1-4$ mHz (periods from 4 to 16 min) at latitudes corresponding to dipole L shells between $L = 6$ and 10. However, the standing SAW frequencies calculated for the dipolar magnetosphere on these L shells are larger by more than an order of magnitude. This problem has been addressed through the use of more realistic magnetic field geometries [*Walker et al.*, 1992; *Rankin et al.*, 2000] that allow for field line stretching in the midnight region [*Waters et al.*, 1996] and by invoking coupling of the SAWs to the slow acoustic mode [*Bhattacharjee et al.*, 1999]. Most recently, *Rankin et al.* [2000] demonstrated that a stretched magnetic topology may be sufficient to explain anomalously low-frequency FLRs. To test this hypothesis, we shall show that the observed FLR frequencies are consistent with optical and magnetometer data that provide information on the geomagnetic field topology of the plasma sheet during intervals when FLRs are observed. In particular, case studies are considered where topology of the inner magnetotail can be modeled from optical data. Then the theoretical FLR spectrum can be computed independently and compared to the observations. The comparison of the theoretical spectrum and the real FLR spectrum validates the modeled magnetic topology. We begin with two experimental case studies of auroral arcs associated with FLRs. These data come from meridian scanning photometers (MSP) and magnetometers from the Canadian Auroral Network for the OPEN Program Unified Study (CANOPUS) array, described in detail by *Rostoker et al.* [1995]; station locations are given in Table 1. The CANOPUS events we consider are on 21 February 1993 and 31 January 1997. Following the experimental study, we apply a simple model

---

[1]Now at Institut de Physique Fondamentale Universite Bordeaux 1, Gradignan, France.

Table 1. CANOPUS Instrument Sites[a]

Location	Station	Geographic Latitude, Longitude	PACE Latitude, Longitude
Eskimo Point	ESKI	61.1, 266.0	71.93, −31.75
Fort Churchill	FCHU	58.8, 265.9	69.72, −30.76
Gillam	GILL	56.4, 265.4	67.38, −30.93
Island Lake	ISLL	53.9, 265.3	64.94, −30.33
Pinawa	PINA	50.2, 264.0	61.16, −31.58
Rankin Inlet	RANK	62.8, 267.9	73.72, −28.97
Taloyoak	TALO	69.5, 266.5	79.65, −36.38

[a] See *Baker and Wing* [1989] for a description of the PACE invariant coordinates.

of the near-Earth magnetotail [*Wanliss et al.*, 2000] to find plausible magnetic field line topologies that existed when FLRs and discrete auroral arcs were observed. Once the magnetic field topology is specified, models of standing SAWs on stretched field lines are considered [*Rankin et al.*, 2000] in order to provide a comparison of the experimental and theoretical FLR spectrum on stretched magnetic field lines.

2. Data and Observations

2.1. The Event of 21 February 1993

[4] The first event study focuses on the FLRs and discrete auroral arcs observed on 21 February 1993. It has been studied previously by *Samson et al.* [1996], who found discrete auroral arcs and FLRs with frequencies of 2.6–2.8 mHz. In this section we include a new analysis of the data and, for completeness, also pertinent details from the work of *Samson et al.* [1996].

[5] The arc system and FLR lasted for >4 hours, from before 0200 to after 0600 UT, when a substorm intensification (expansive phase onset) occurred. Figure 1 shows the gray scale plots of meridian scanning photometer (MSP) data from the Gillam station, located at $67.4°, −31.0°$ Polar Anglo-American Conjugate Experiment (PACE) latitude and longitude. The raw data come in the form of north-south scans of intensity as a function of elevation angle. All the MSP plots in this paper scale the angles from the observer to the maximum of intensity to the assumed altitude of 110 km for the 486.1-nm wavelength and 230 km for the 630.0-nm wavelength. The H_β (486.1 nm) are in Figure 1a and the 630.0 nm emissions are in Figure 1b. Figures 1a and 1b include the equatorward boundaries of the region of diffuse emissions overlaid as a thick white line. These boundaries are used to model the magnetic topology and will be discussed in that context in section 3. The H_β data in Figure 1a show the signature of energetic ion precipitation (tens of keV) at the equatorward edge of the auroral oval. Diffuse 630.0-nm emissions (Figure 1b) reflect the precipitation produced from low-energy electrons (hundreds of eV).

[6] The auroral arc and the optical oscillations associated with the FLR are very clear as the region of higher emission intensity in the 630.0-nm emission (Figures 1b and 2). The arcs are shown in Figure 1 of *Samson et al.* [1996]. Although it is not clear in this gray scale plot (Figure 1b), there are also 630.0-nm emissions at higher latitudes which correspond to the diffuse emissions associated with the electron plasma sheet [*Samson*, 1994]. The diffuse emissions are much lower in intensity than the

oscillating arc and are not easy to see in the gray scale image, but they are visible in the inset, which shows the intensity versus latitude at three times; the equatorward boundaries of the diffuse emissions are indicated by the arrows. In the main part of Figure 1b this lower edge of the diffuse aurora is indicated by the solid white line calculated using a Canny edge detection routine [*Canny*, 1986], which is capable of detecting weak edges. This edge detection routine finds edges by looking for local maxima of the gradient of the optical data. Whereas the oscillating auroral arc occurs around $66.3°$ for the 630.0-nm emissions, the equatorward edge of the region of diffuse emissions from low-energy precipitating electrons occurs poleward of $69°$. Figure 2 shows a time series of the 630.0 nm MSP data, taken at a latitude of $66.3°$. Now the oscillations in luminosity associated with the pronounced brightening of the arc structure after 0500 UT are very clear. The power spectrum of the MSP data (Figure 3) shows a pronounced spectral peak around 2.4 mHz. All power spectra are computed by detrending the data with a linear trend and high-pass filtering with a fourth-order time domain Butterworth filter with an edge at 0.5 mHz. The power spectra are then computed from the discrete Fourier transform of this signal. *Samson et al.* [1996] used all-sky imager data to show that the latitudinal center of the FLR moved slightly poleward at this time, possibly indicating a small dipolarization of the field lines threading the FLR and auroral arcs. Their Figure 9 shows how at ∼0520 UT the arcs dimmed, observed electron energies were several hundred eV, and large-scale, auroral vortex structures appeared in the all-sky imager data.

[7] The *X* component magnetometer data for CANOPUS stations (approximately north-south geomagnetic for these locations), measured every 5 s, show evidence for pulsation activity (∼2.4 mHz) during the interval from 0200 to 0430 UT. At 0520 UT, enhanced Pi2 activity is clearest and coincident with the strongest brightenings in the periodically modulated auroral arc [*Samson et al.*, 1996, Figure 11].

[8] Modeling of this event, which is discussed later, requires estimation of the energy of the low-energy precipitating electrons in the diffuse aurora mapping to the plasma sheet. Through use of the 557.7/630.0 nm line ratios, as described by *Daniell and Strickland* [1986] and *Strickland et al.* [1989], the energies of the precipitating electrons corresponding to the pulsating arc were ∼2 keV, while the diffuse aurora is associated with several hundred eV precipitating electrons.

2.2. Event of 31 January 1997

[9] The second event in our study has previously been discussed but in a different context [e.g., *Lotko et al.*, 1998; *Lund et al.*, 1999]; thus our discussion here focuses on new aspects of the event. Figure 4 shows the photometer data for 486.1-nm and 630.0-nm emissions. As before, the equatorward borders of the diffuse H_β and 630.0-nm emissions are overlaid as solid white lines. The equatorward border of the 630.0-nm emissions occurs around $71°$, which is poleward of the pulsating arcs near $68°$. Pulsations in the auroral arc are clearly visible in Figure 5, which shows a time series of the 630.0-nm MSP data, taken at a constant latitude of $68.4°$. The resonance structure observed after ∼0410 UT has large amplitude and is >100 R above the emission
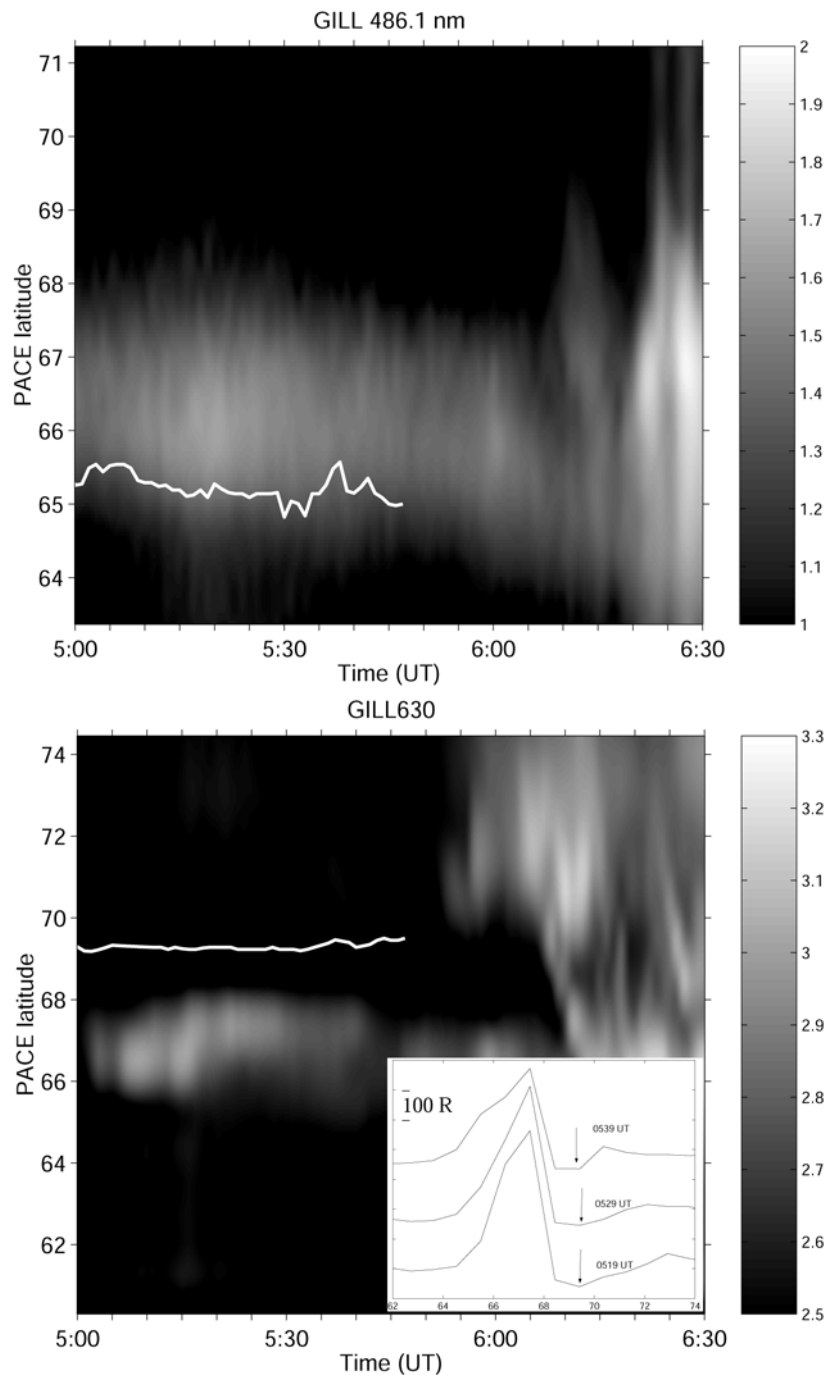
Figure 1. Meridian scanning photometer data from the GILL station in the (a) 486.1-nm and (b) 630.0-nm wavelengths on 21 February 1993. The equatorward boundary of the diffuse emissions are shown as a solid white line. The inset in Figure 1b shows the 630.0-nm emission intensity versus latitude at three different times; the arrows indicate the location of the equatorward edge of the diffuse emissions. PACE coordinates are explained by *Baker and Wing* [1989].

intensity in the interval 0300−0400 UT. The power spectrum of this time series, shown in Figure 6, is fairly monochromatic with a dominant peak at 1.4 mHz and a smaller peak at 2.3 mHz. Unlike the previous event where the pulsating arcs occurred prior to expansive phase onset, here the pulsating arcs are observed some time after a substorm expansive phase at 0244 UT.

[10] The X component magnetometer data for CANO-PUS stations are shown in Figure 7. The traces show a substorm bay signature around 0300 UT and evidence of pulsation activity throughout the given time interval. Figure 8a shows the power spectrum of the X component of GILL in the interval from 0400 to 0500 UT during which time the pulsating arcs are clearest in the 630.0-nm MSP
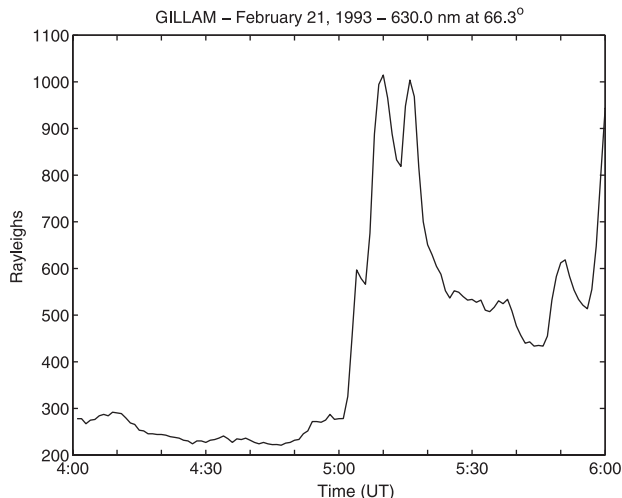
Figure 2. Time series of 630.0-nm MSP data from GILL taken at 66.3° latitude. Note the strong luminosity oscillations between 0500 and 0600 UT.

data. The strongest peak in power is visible at ~1.3 mHz, and there is a slightly smaller peak at ~1.9 mHz. Figure 8b is the high-pass filtered X component data from the GILL station between 0400 and 0500 UT.

3. Modeling the Near-Earth Magnetotail Configuration

3.1. Modeling Technique

[11] Our method of evaluating the magnetic field topology stems from the observations of low-altitude isotropy boundaries of precipitating particles. The concept of using the isotropy boundaries for remote sensing of the magnetotail topology was first introduced by *Sergeev and Malkov* [1988] and further developed by others [*Sergeev et al.*, 1993a; *Pulkkinen et al.*, 1991, 1992, 1998; *Kubyshkina et al.*, 1999]. The technique relies on the inference that the isotropy boundaries of precipitating particles observed at low altitudes correspond to the boundaries between adiabatic and nonadiabatic regimes of particle motion in the equatorial current sheet region. Scattering out of the current sheet depends on the equatorial magnetic field and is also sensitively dependent on the gyroradius of the particle. The theory of scattering out of the plasma sheet and subsequent precipitation has been described in numerous other papers [*Büchner and Zelenyi*, 1987; *Zelenyi et al.*, 1990; *Liu et al.* 1998]. Basically, when there exist significant magnetic field variations on the scale of the particle gyroradius, non-adiabatic behavior occurs, with the result of scattering out of the plasma sheet. The κ parameter, defined by *Büchner and Zelenyi* [1987], is useful in characterizing the non-adiabatic particle behavior. The parameter is defined by

$$\kappa = \sqrt{\frac{R}{\rho}}, \tag{1}$$

where R is the magnetic field line radius of curvature and ρ is the particle gyroradius measured in the current sheet region. The dependencies in κ show that the type of particle

motion (namely, adiabatic and nonadiabatic or chaotic) is dependent on both the magnetic field geometry and particle energy. In Figure 9 an example is shown comparing dipole field lines to stretched field lines. Two stretched cases are shown, with different current sheet thicknesses, as measured at 10 R_E. The field line radius of curvature is smaller for thin current sheets, implying that particles of the same energy will be more easily scattered from thin current sheets than from thicker current sheets.

[12] *Sergeev and Malkov* [1988] and *Delcourt et al.* [1996] demonstrated, through test particle simulations, that for approximately $\kappa < 3$, particle motion is nonadiabatic and particles are scattered out of the current sheet region, a significant portion of which can enter the loss cone and subsequently precipitate into the ionosphere [*Lyons and Speiser*, 1982; *Liu et al.*, 1998]. For larger values of κ the behavior is adiabatic and results in trapped particle distributions at low altitudes. Thus in the magnetotail, there exists a separatrix between the different types of particle behavior. Because the radius of curvature is typically larger in the near Earth, κ tends also to be larger there, becoming smaller with distance downtail; in the distant tail, $\kappa \ll 1$. On the other hand, close to the Earth where the dipole field is stronger, the parameter κ can be much larger than unity, and the particle motion is adiabatic. In between, at the transition between tail-like and dipole-like field configurations, plasma sheet particles can have variable κ values. In this paper we define the $\kappa = 3$ separatrix as the boundary between adiabatic and nonadiabatic particle behaviors. Tailward of the separatrix, pitch angle scattering occurs, and particles are ejected from the current sheet region, some of which enter the loss cone. Here, therefore, distribution functions have a loss cone that is completely filled, and low-altitude satellites will observe isotropic distribution functions. Trapped particle distribution functions occur earthward of the $\kappa = 3$ separatrix. This very distinct boundary has been observed, and the model of scattering out of the current sheet provides a generally accepted explanation for the observations of low-altitude ion [*Sergeev et al.*, 1993a; *Newell et al.*, 1998] and electron [*West et al.*, 1978; *Sergeev et al.*, 1994] distribution functions.
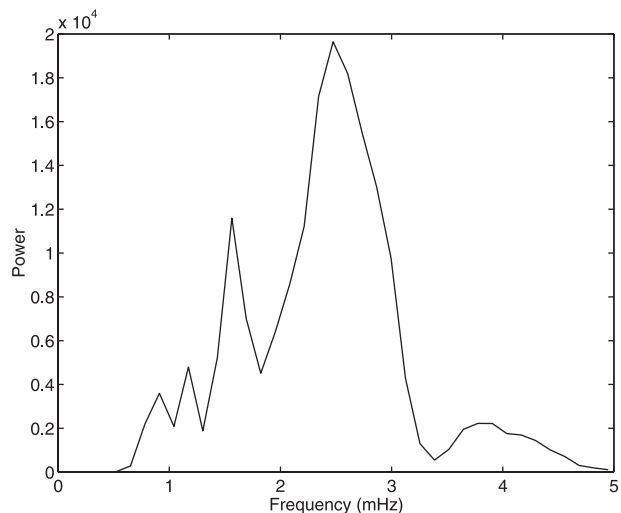
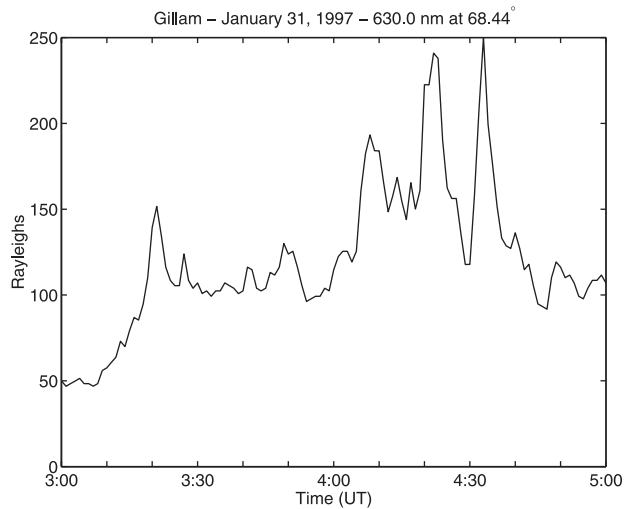**Figure 3.** Power spectrum of the time series in Figure 2.
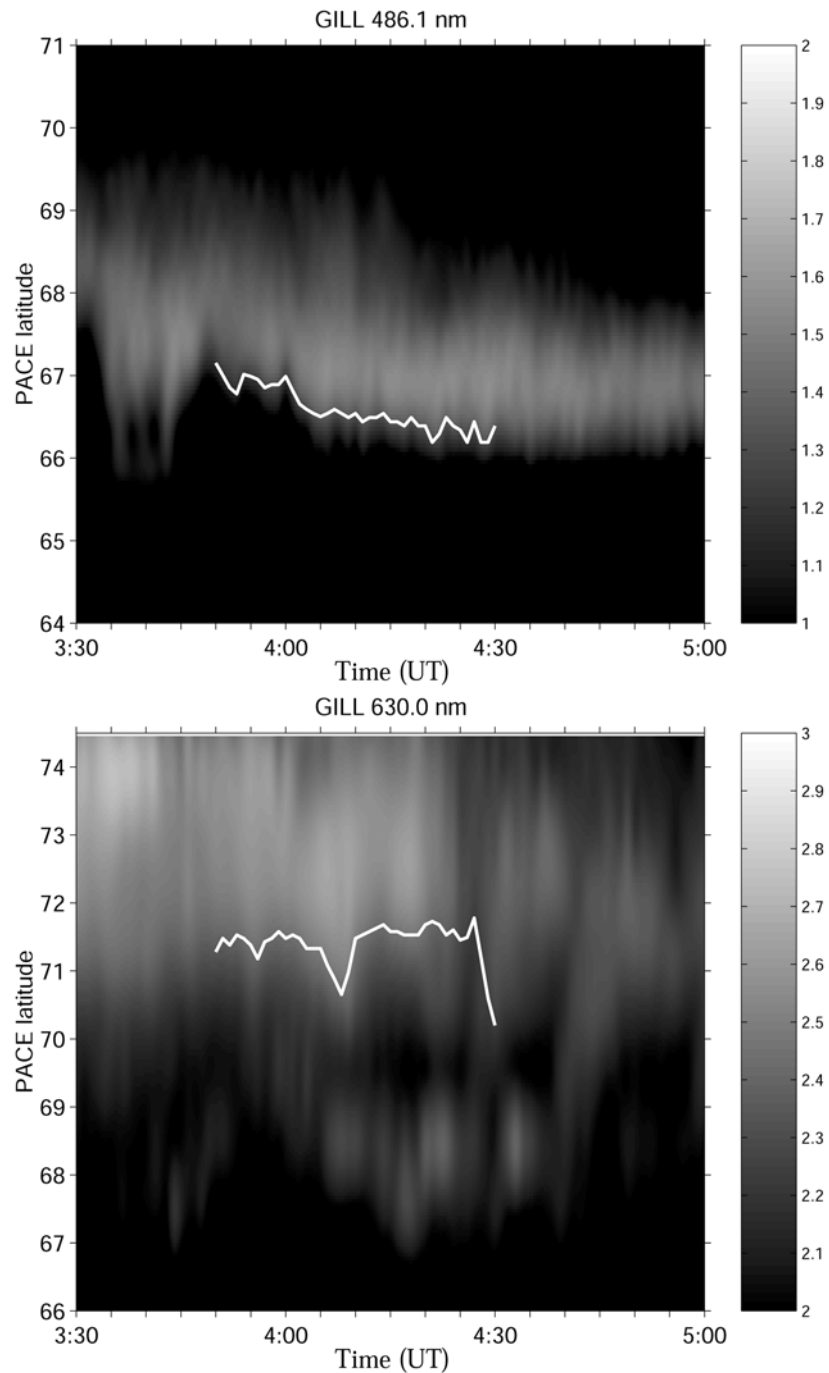
Figure 4. Meridian scanning photometer data from the GILL station in the (a) 486.1-nm and (b) 630.0-nm wavelengths on 31 January 1997. The equatorward boundary of the diffuse emissions are shown as a solid white line. PACE coordinates are explained by *Baker and Wing* [1989].

[13] The original aspect of our work here is that we have extended the isotropy boundary idea to include the ground observations of the meridian scanning photometers. Both the H$_\beta$ (486.1 nm) and 630.0-nm emissions result from the precipitation of particles whose energies are fairly well established. Precipitating ion energies for H$_\beta$ average ∼20 keV [*Samson et al.*, 1992] but can vary from a few keV to over 100 keV. The electron energy range is determined on the basis of the 557.7/630.0 nm line ratios [*Daniell and Strickland*, 1986; *Strickland et al.*, 1989] and averages a few

hundred eV but can range from 100 eV to sometimes above 1 keV. Equatorward borders of the diffuse H$_\beta$ and 630.0-nm emissions form a sharp boundary delineating the ionospheric regions between isotropic precipitating particle and trapped particle distributions [*Samson*, 1994]. Thus we are able to make a direct connection between the remote magnetic topology and the MSP data.
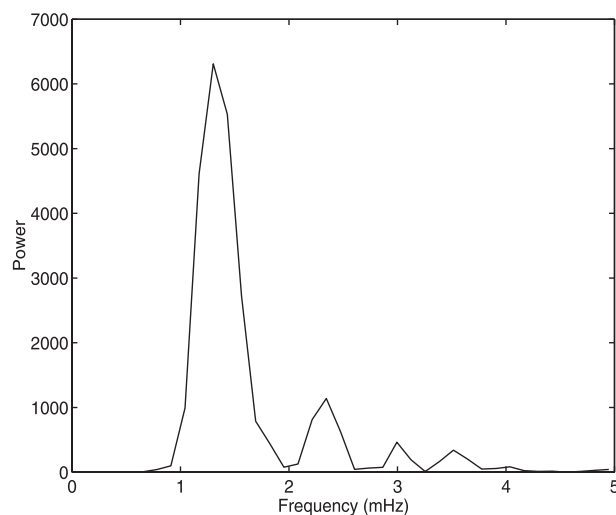
[14] *Wanliss et al.* [2000] used a simple magnetic field model with variable crosstail current thickness to successfully model MSP observations during substorm growth
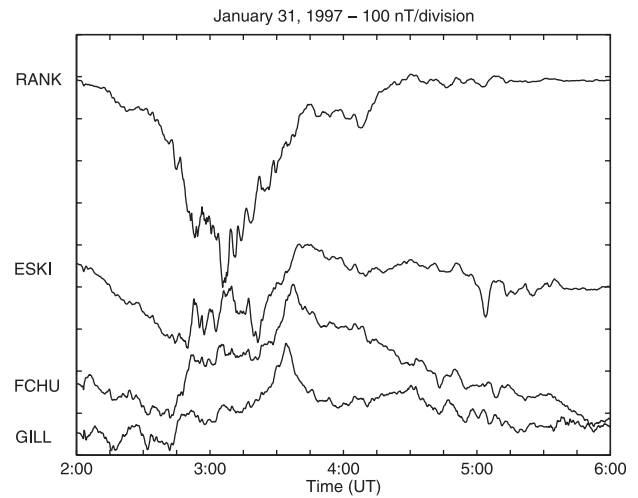
Figure 5. Time series of 630.0-nm MSP data from GILL taken at 68.4° latitude.

Figure 7. Magnetic X component from the Churchill line of magnetometers. Local magnetic time is approximately UT minus 6 hours. The magnetic declination of all these stations is $\sim 3°$ or less, and consequently, the X component is approximately magnetic north-south.

phase. Their technique was to find the location in the model neutral sheet where the isotropy boundary was observed (i.e., $\kappa = 3$) and then to map this point along the magnetic field line into the ionosphere. There the latitude of the field line is compared to the actual latitude of the MSP observation. The only parameter in their model which was allowed to vary was the crosstail current sheet thickness; other parameters such as lobe field strength were kept constant. In our present paper the practice is to select particle energies in the plasma sheet and to find the $\kappa = 3$ boundary for both electrons and protons. These boundaries are then subsequently mapped to the ionosphere along magnetic field lines. Ideally, model parameters can be varied until the $\kappa = 3$ boundary corresponds to the appropriate equatorward edges of the auroral emissions.

[15] Whereas *Wanliss et al.* [2000] considered only protons, in this paper we extend the modeling to include also the equatorward border of the 630.0-nm emissions due to precipitating electrons. The constraints on the magnetic field model are made more robust through inclusion of the

equatorward boundary of the 630.0-nm emissions because it reduces somewhat the choice of models that fit the observations. The fitting algorithm begins with the time series calculation of the equatorward borders of the H_β and 630.0-nm MSP data. These borders are overlaid as white lines on the MSP data in Figures 1 and 4. The error in calculation of the 486.1-nm border is $\pm 0.25°$ and is $\pm 0.5°$ for the electrons. The least squares fitting routine is essentially the same as before [*Wanliss et al.*, 2000], with the exception that now the electron borders are included. The magnetic field model is used, and its free parameters are varied, so that a matrix of separatrix locations are found between adiabatic and nonadiabatic motion in the magnetotail (corresponding to $\kappa = 3$). Next, these positions are mapped to their latitudinal location in the ionosphere and compared to the actual location of the ionospheric isotropy boundaries, calculated previously from the MSP

Figure 6. Power spectrum of the time series in Figure 5.
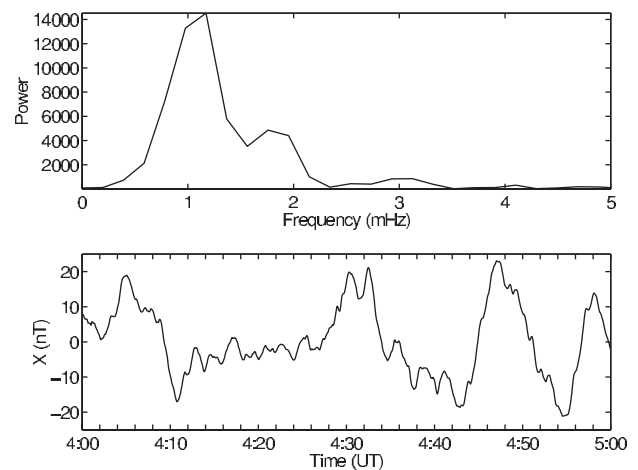
Figure 8. (a) Power spectrum of the GILL station between 0400 and 0500 UT. (b) The high-pass-filtered X component from GILL.
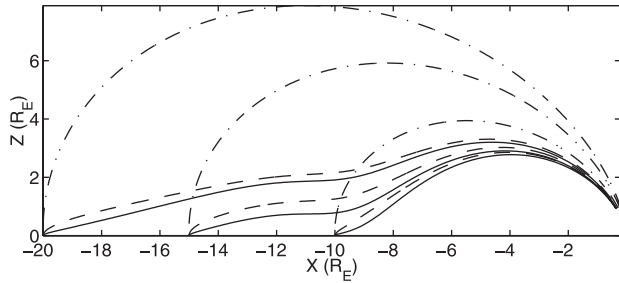
Figure 9. Model magnetic field lines in the noon-midnight meridian with two different current sheet thicknesses (solid and dashed lines) are compared to the dipole field (dot-dashed line).

data. Since the model boundary locations depend on the energies of the electrons and protons, as well as on the magnetic field topology, the fitting procedure at a certain time, t, is obtained from the minimization of the following statistic:

$$\epsilon(t) = \sum_{E_p} \sum_{E_e} \sum_{L_z} [\theta_{MSP}^p(t) - \theta^p]^2 + [\theta_{MSP}^e(t) - \theta^e]^2, \quad (2)$$

where $\theta_{MSP}^{p/e}$ are the latitudinal locations of the actual $H_\beta/630.0$ nm equatorward boundaries calculated from the MSP data and $\theta^{p/e}$ are the model locations based on the mapping of the isotropy boundary from the magnetotail to the ionosphere. The modeled precipitation latitudes are dependent on the model parameters, for example, current sheet half thickness L_z and also the proton/electron energy in the plasma sheet, $E_{p/e}$. Degrees of complexity may be introduced through the addition of more parameters or use of more elaborate models.

3.2. Magnetotail Topologies

[16] We attempt to fit the MSP data via a simple parametric model of the magnetotail. The model we use was introduced by *Wanliss et al.* [2000] to approximate the topology of the inner magnetotail during the substorm growth phase, and we include pertinent details here. It comprises a dipole field, a tail component, and an azimuthally and radially confined weak magnetic field region (WFR). All three modular components are used to build up the final magnetic field model configuration. The WFR creates a region of minimum B in the near-Earth plasma sheet. Figure 1 of *Wanliss et al.* [2000] (not shown here) gives a profile of our model magnetic field in the current sheet, compared to observations, and shows the region of minimum B. The WFR is located around 11 R_E to be in accord with observations [*Kaufmann*, 1987; *Baker and McPherron*, 1990; *Iijima et al.*, 1993; *Baker et al.*, 1993; *Sergeev et al.*, 1990, 1993b; *Nakai et al.*, 1997]. The tail component is the *Zwingmann* [1983] two-dimensional equilibrium which is a daughter of the earlier *Harris* [1962] equilibrium. For this component the most important parameters are the lobe field and the cross-tail current thickness. Figure 10 shows the model lobe field compared to satellite observations [*Slavin et al.*, 1985; *Nakai et al.*, 1991]. We fixed the lobe field parameter to achieve a qualitative fit to the satellite observations. However, the current sheet thick-

ness parameter was not fixed but allowed to vary in the modeling procedure.

[17] Since our model was initially designed for substorm growth phase, or other times when the magnetotail is more stretched than average, its utility for different intervals may be questioned, and we now draw attention to its limitations. In order to describe the application of our technique to quiet conditions we refer to an event study; namely, the 9 February 1995 substorm previously considered in detail [*Wanliss et al.*, 2000; *Friedrich et al.*, 2001]. This event is unique in that it presents a case where prior to the substorm the magnetosphere was as close to a low-energy, or "quiet," state as is likely to be possible. Our present magnetic field model was used successfully to model the 9 February 1995 growth phase which commenced at ∼0335 UT [*Wanliss et al.*, 2000]. However, we were also able to model the field prior to the growth phase, for example, around 0330 UT, which was when magnetic activity was negligible. At this time the 630.0-nm and H_β equatorward boundaries were at 70.0° and 67.5°, respectively (these data shown in Figure 1 of *Friedrich et al.* [2001] are not reproduced here). Thus our magnetic field model appears able to fit topologies not only during intervals when the magnetotail is extremely stretched but also during relatively quiet intervals.

[18] One way to quantify the range of applicability of our model is to find the latitudinal extent over which it is able to predict the isotropy boundary location in the ionosphere. Figure 11a shows, for several energies of precipitating particles, the range of latitudes for which the model is able to predict isotropy boundaries. Isotropy boundaries are shown for three proton and electron precipitating energies, namely, 10, 20, and 80 keV and 100, 300, and 1000 eV, respectively. The solid curves are for the protons, and the dashed curves are for the electrons, with the higher-latitude curves corresponding to the lower energies. For each energy of precipitating particles the current sheet thickness in our model is varied, resulting in a range of different latitudes for the predicted isotropy boundaries. Figure 11a shows that the isotropy boundaries move equatorward as the current sheet thins, which corresponds to a stretching in the magnetotail.
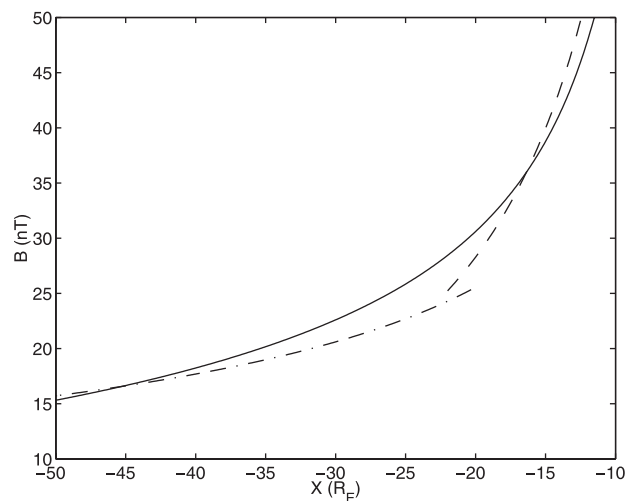
Figure 10. Model lobe field (solid) calculated at $(Y, Z) = (0,10)$ R_E is compared to the observations of *Slavin et al.* [1985] (dot-dashed) and *Nakai et al.* [1991] (dashed).
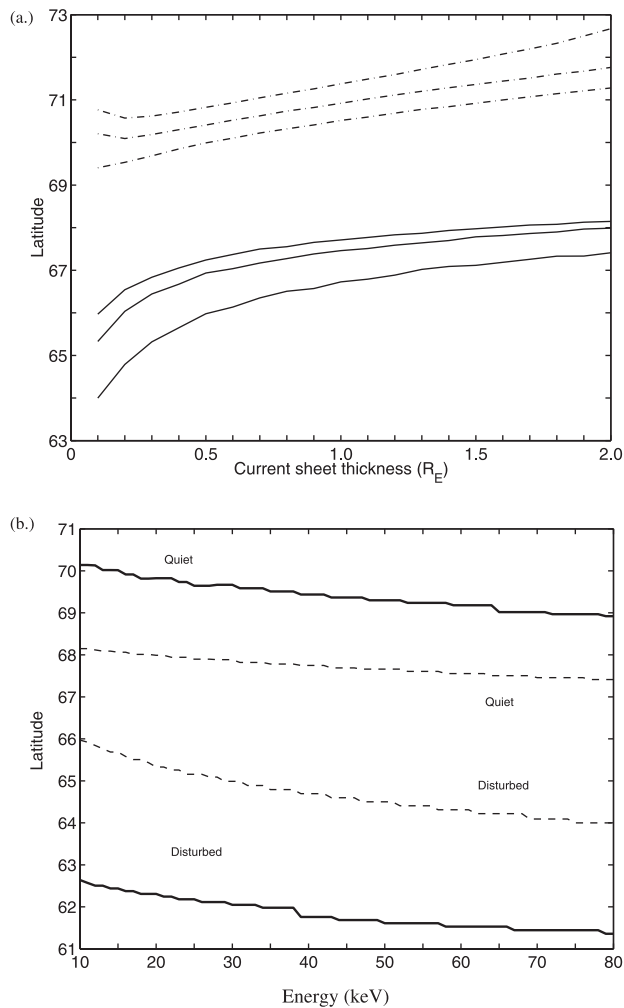
Figure 11. (a) Comparison of the ionospheric latitudes where our new model is able to predict the locations of isotropy boundaries. The independent variable is the model cross-tail current sheet thickness. The solid lines show the boundaries for protons of energy 10, 20, and 80 keV, and the dashed lines show the boundaries for electrons of energies 100, 300, and 1000 eV. The highest-latitude curves correspond to the lowest energies. (b) Isotropy boundaries only for protons for variable energies. A comparison is made between our model (dashed curves) and the T96 model (solid curves) for "quiet" and "disturbed" situations. The quiet situation for our model corresponds to a current sheet 2 R_E thick, and for the disturbed interval we used 0.1 R_E. For T96 we used solar wind dynamic pressure of 0.5/5 nPa, $Dst = 5/-40$, $B_y = 0$, $B_z = 5/-5$ nT for the quiet and disturbed cases, respectively.

As well, for reasonable ranges of energies of precipitating particles associated with aurorae, Figure 11a indicates that the model will fail when the H_β isotropy boundary is poleward of ∼68° and the electron boundary is poleward of ∼73°. For the 9 February 1995 event, mentioned above, the electron boundary is always within the range of the model, but the proton boundary, prior to growth phase, occasionally reaches as high as 69°. Thus we have reason to believe that the model will sometimes be inappropriate for use during extremely quiet intervals. However, the general

technique of inverting the isotropy boundary data remains valid, and another model suited to quiet times might be used with success. During times of extreme activity, such as expansive phase onset, the boundaries can also be outside of our modeling range, and the model should not be used.

[19] As mentioned above, more elaborate models might be appropriate when ours fails. Figure 11b shows a comparison of the T96 model and ours with the predicted latitude of the H_β isotropy boundaries versus energy for precipitating protons. The solid curves are for T96, and the dashed curves are for our model. Shown in Figure 11b are "quiet" and "disturbed" results. For our model the quiet case corresponds to a current sheet that is 2 R_E thick and the disturbed case corresponds to a current sheet that is 0.1 R_E thick. The curves indicate a narrow range of applicability; when the isotropy boundaries for protons fall between ∼68° and 64°. For T96 we used solar wind dynamic pressure of 0.5/5 nPa, $Dst = 5/-40$, $B_y = 0$, $B_z = 5/-5$ nT for the quiet and disturbed cases, respectively. The quiet case corresponds to large and steady northward interplanetary magnetic field and very small solar wind ram pressure. The disturbed case corresponds to conditions that can exist during magnetic storms and magnetospheric substorms. Because of the number of inputs into T96 these curves are not unique and represent only a sample of results that correspond to quiet or disturbed intervals. However, they do provide an idea of the range over which one might apply our techniques if a model such as T96 were suitably constrained for the inversion problem. Clearly, at least for precipitating protons, T96 easily encompasses quiet times, whereas our model should be used with care during quiet times and will sometimes be inappropriate. Corresponding electron curves are not shown; for the disturbed case, T96 predicted electron isotropy boundaries above 74°, and low-energy electron isotropy boundaries did not exist within the T96 magnetosphere for the quiet case (i.e., $\kappa > 3$ always). This seems to indicate the insufficiently stretched nature of T96, particularly in the near-Earth region; MSP observations for 630.0 nm during growth phases (i.e., disturbed case) show that the diffuse emissions tend to reach several degrees equatorward of 74°, and emissions are certainly present during quiet times, although T96 does not predict their existence for the parameters we chose. This confirms previous studies which show that possibly because of their statistical nature the *Tsyganenko* [1987, 1989, 1995, 1996] magnetotail models tend not to be sufficiently stretched [*Fairfield*, 1991; *Sergeev et al.*, 1993a, 1994; *Pulkkinen et al.*, 1991, 1992, 1998, 1999; *Lu et al.*, 1999; *Kubyshkina et al.*, 1999]. Although our model is limited, in this paper the observational MSP data show events during which the H_β move equatorward, thus giving us the reasonable expectation that stretching is occurring in the magnetotail. Furthermore, both modeled events also have isotropy boundaries of latitudinal extent that makes them amenable for study via our simple magnetic field model.

3.3. Modeling Results

[20] The event of 21 February 1993 is modeled from 0500 to 0550 UT during an interval when clear storage of energy occurs in the magnetotail. After 0600 UT (Figure 1), there were repeated brightenings and poleward motions of the aurora, indicating a release of energy, and relaxation to a
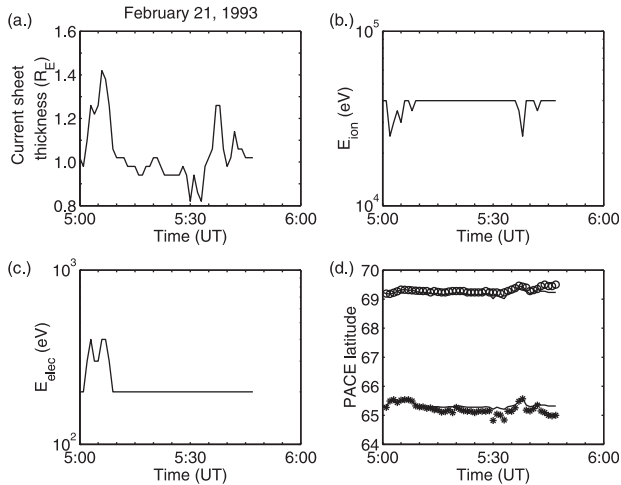
Figure 12. The 21 February 1993 statistics calculated through the modeling process. (a) Current sheet thickness at 10 R_E, (b) ion energy, (c) electron energy, and (d) best fit comparison shown as the solid line to the actual 486.1/630.0 nm equatorward boundaries (stars and circles, respectively).

less stretched state. Figure 12 shows the best fit statistics and results for 21 February 1993. The model fit was attempted between 0500 and 0550 UT, and on the basis of the line ratios we used electron energies of 200–400 eV, as well as ion energies between 20 and 40 keV, in the minimization routine. Figure 12a shows the variation of current sheet thickness during this interval. These variations are in response to the small poleward and equatorward motions of the electron and proton borders (Figure 12d). The model current sheet reaches a maximum thickness, measured at $X = -10$ R_E, of just over 1.4 R_E by 0510 UT, after which the model predicts a thinning to ∼0.8 R_E at 0515 UT. This thinning trend was also previously observed for other modeled growth phases [*Wanliss et al.*, 2000]. The current sheet thickens again at the end of the modeling interval. Goodness of the fit between the model and MSP borders is determined from Figure 12d. Here the actual equatorward proton and electron borders, measured from the MSP, are shown as solid lines, with the proton border being equatorward of the electron border. The best fit model-predicted borders are overlaid as circles/stars for the electrons/protons. These data show that the fit is very good throughout the modeling interval.

[21] Figure 13 shows the statistics for the event on 31 January 1997, fitted between 0350 and 0430 UT. During the interval, brightening and equatorward motion of the diffuse aurora occurred, indicating energy input and stretching of the magnetotail. A small poleward expansion (not shown) occurred at 0645 UT which indicates relaxation to a less stretched configuration. For this case the electron energy range is slightly lower, 100–200 eV, and the ions have higher energies; 60–80 keV. Figure 13a shows the variation of current sheet thickness during this interval. From 0350 to 0408 UT the current sheet gradually thins from ∼2.0 R_E to 1.0 R_E and then thickens again to 1.7 R_E between 0412 and 0428 UT. Between 0428 and 0430 UT, there is rapid thinning to ∼0.9 R_E. Goodness of the fit between the model borders and MSP borders is determined from Figure 13d.

As before, the actual equatorward proton and electron borders are shown as solid lines, and the best fit values are shown as circles and stars for the electrons and protons, respectively. Through much of the fitting interval there is some variation between the best fit latitudes and the MSP data, although the fit achieved is still within the error range.

4. Comparison With FLR Models

[22] The previous sections have demonstrated the modeling effort to fit plausible magnetic topologies to the MSP data in the ionosphere. Although this approach is relatively simple, it appears to produce reasonable results [*Wanliss et al.*, 2000]. In this section a stretched magnetic field line model in the vicinity of the midnight region [*Singer et al.*, 1981] will be utilized to compare the expected FLR eigenmodes that are excited on the magnetic field lines which have been determined from the modeling. The eigenmode equation for standing SAWs in fields with arbitrary topologies is

$$-\omega^2 S = \frac{h_\phi}{h_\psi} \partial_l V_A^2 \frac{h_\psi}{h_\phi} \partial_l S, \qquad (3)$$

where $S(l)$ is the field-aligned SAW eigenfunction at a given magnetic L shell, $V_A(l) = B_0/\sqrt{\mu_0\rho}$ is the local Alfvén velocity, l is the coordinate along the magnetic field line, and h_ϕ, h_ψ are the metric coefficients describing the magnetic field topology. The validity of equation (3) is discussed fully by *Tikhonchuk and Rankin* [2000]. Here we will note only that small second-order terms (of order $\nabla_\perp^2$) that represent small corrections to the eigenfrequencies have been neglected.

[23] In order to calculate the SAW eigenfrequency from equation (3), we use the parametric definition of the magnetic field line: $R(\theta)$ and $B_0(\theta)$, where R is the distance from the Earth center to a point of the magnetic field line and B_0 is the corresponding parallel magnetic field. Then the metric
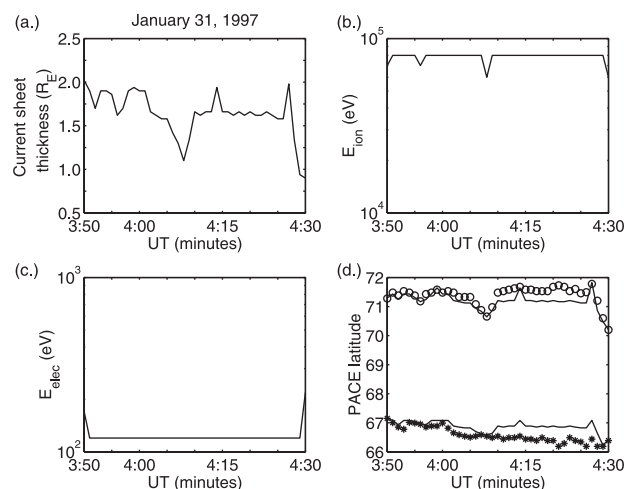
Figure 13. The 31 January 1997 statistics calculated through the modeling process. (a) Current sheet thickness at 10 R_E, (b) ion energy, (c) electron energy, and (d) best fit comparison shown as the solid line to the actual 486.1/630.0 nm equatorward boundaries (stars and circles, respectively).

February 21, 1993

(a.)

January 31, 1997

(b.)
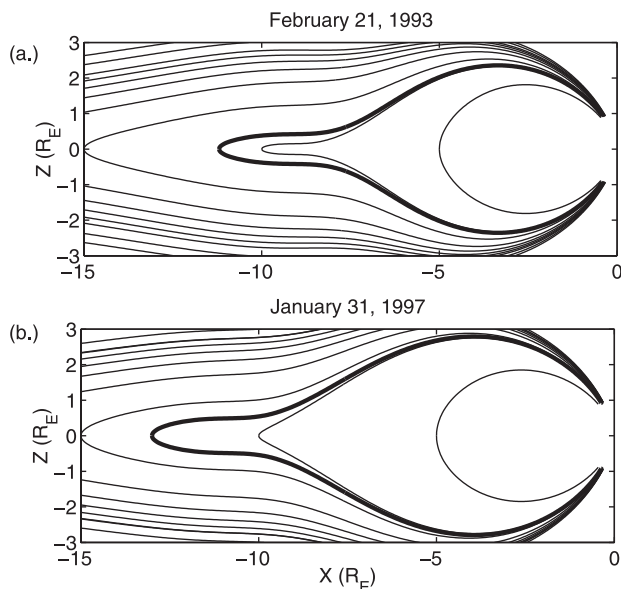
Figure 14. Modeled magnetic field topologies for (a) 21 February 1993 and (b) 3 January 1997 at a moment when FLRs are observed in the optical data. The thick dark line indicates the magnetic field line used to compute the predicted eigenfrequency.

coefficients are defined as $h_\phi = R \sin \theta$ and $h_\psi = (B_0 h_\phi)^{-1}$, and the field-aligned coordinate has been found from

$$dl/d\theta = \sqrt{R^2 + (dR/d\theta)^2}, \qquad (4)$$

where $l = 0$ in the equatorial plane.

[24] For the purposes of comparison, it is necessary to select appropriate plasma densities in the plasma sheet and in the ionosphere. Accordingly, we consider a two-species plasma comprising hydrogen in the plasma sheet and a cold oxygen component of atmospheric origin with a density $n_0 = 10^4$ cm^{-3} at the ionospheric ends that decreases exponentially with altitude over a scale length $h_O = 600$ km. The density profile is given by

$$n(l) = n_H + n_O e^{-(l_{\max} - |l|)/h_O}, \qquad (5)$$

where n_H is the hydrogen density in the plasma sheet. This profile reproduces a characteristic peak of the Alfvén velocity at an altitude of $10,000 - 15,000$ km. The ionosphere is assumed to be highly conducting, and a finite Pederson conductivity ($\Sigma_P = 10$ S) is allowed for the purposes of consistency.

[25] The parameter that remains to be selected is the hydrogen (proton) density in the plasma sheet. Once this is known, we will be able to compare the observations with the FLR model on stretched field lines and to provide a further test of the magnetic field topology fitted using the analytical model and MSP data. For the plasma sheet earthward of 25 R_E, *Huang and Frank* [1986] used ISEE 1 data, for all activity levels, to find densities of $n_H = 0.5$, 0.29, 0.23 cm^{-3} for dawn, midnight, and dusk regions. Similarly, *Baumjohann et al.* [1989] found averaged *PS* measurements of $0.15-0.45$ cm^{-3}, and *Lennartsson and*

Shelley [1986] and *Lennartsson* [1992] reported that the *PS* average ion density ranges from 0.4 to 1 cm^{-3}. A more recent study by *Borovsky et al.* [1998] measured the density in the equatorial current sheet region between 17.5 and 22.5 R_E and found that it typically ranged from <0.1 cm^{-3} to slightly more than 1 cm^{-3}. In the FLR modeling, we use a density of 1 cm^{-3} as a reference point.

[26] We apply the model to the two events we have studied thus far. For the 21 February 1993 event the FLR eigenmode frequencies are computed along the magnetic field lines that map to the center of the auroral arc, at ∼66.3°. This field line is indicated by the thick trace in Figure 14a, along with other representative field lines. The observed frequency for the resonance structure in the auroral arcs has $f \sim 2.6-2.8$ mHz. When we apply the above theoretical model, we find frequencies around 3 mHz are achieved for $n_H = 1$ cm^{-3}. We find that lower frequencies require a thinner current sheet and/or higher density (2 cm^{-3} gives $f \sim$ 2.1 mHz). For the 31 January 1997 event, with pulsating arcs with $f \sim 1.4$ mHz, the appropriate fitted field lines are shown in Figure 14b. For this case, $n_H = 1$ cm^{-3} is needed to get frequencies around 2 mHz (2 cm^{-3} gives $f \sim 1.4$ mHz). It is clear that the modeled frequencies are comparable to the observations provided there is field line stretching in the range of the L shells covering the observations. In the absence of field line stretching, the eigenfrequencies are larger than our estimates by an order of magnitude.

5. Discussion

[27] We have further developed previous techniques [*Wanliss et al.*, 2000] to model the magnetic field of the inner magnetotail during the time of observation of FLRs. Whereas previously only the H$_\beta$ data were used to constrain the magnetotail model, the model is now made more robust through the use of the additional constraint of the equatorward border of the 630.0-nm emissions. The equatorward boundary of the H$_\beta$/630.0 nm emissions corresponds approximately to the inner edge of the proton/electron plasma sheet, respectively [*Samson*, 1994]. In terms of precipitating particle fluxes these photometric boundaries mark the separatrix between isotropic and trapped distribution functions.

[28] In this paper, we have analyzed observations of low-frequency FLRs and pulsating auroral arcs and made comparisons with the predictions of simple models. We have estimated the magnetic field topology in the region where FLRs are observed and calculated the FLR spectrum on specified stretched geomagnetic lines. This is accomplished by using CANOPUS optical data as a proxy for ion and electron precipitation that can be mapped into the changing topology of the near-Earth magnetotail during the observation of FLRs. The topology modeling technique comes with a few caveats. The present simple magnetic field model is not likely to be applicable during very quiet magnetospheric intervals when minimal stretching occurs in the magnetotail. Similarly, it will fail to model plausible topologies during extremely disturbed intervals such as substorm expansive phase onset or recovery. Thus our model is best suited for weakly to moderately disturbed intervals, or intervals when some equatorward motion of H$_\beta$ is observed. Another caveat is that our simple model only attempts to approximate

topology in the near-Earth region. An important next step would be to apply the technique through the use of more elaborate global magnetic field models, although this would introduce additional modeling complexity as the number of free model parameters increase. One way to improve the situation is to include more data and thus reduce ambiguities [*Kubyshkina et al.*, 1999]. Aside from the addition of in situ satellite magnetic field data, it may be possible to use the input from several MSPs, rather than from one only. Such an ambitious goal may certainly be feasible, for example, through use of the CANOPUS chain of MSPs.

[29] Since we were able to specify a model magnetic field topology on which FLRs exist, it was possible to compare the real data with the FLR model for stretched field lines [*Singer et al.*, 1981; *Rankin et al.*, 2000]. In this manner, we provided a comparison of the experimental and theoretical FLR spectrum on stretched magnetic field lines. The two model approaches we have considered, namely, the topology mapping and FLR eigenfrequency spectrum calculation, provide independent checks on one other. They confirm that the diffuse aurora and FLRs observed lead to a modeled FLR spectrum consistent with standing shear Alfvén waves that are excited on field lines that are stretched (from a dipole) in the near-Earth region of the plasma sheet. The model eigenfrequencies were found to be sensitive to the degree of stretching of the magnetic field lines. The proton number density (n_H) is an important parameter in the FLR model, but it turns out that the eigenfrequencies are not as sensitive to n_H as they are to the stretching; factor of 2 differences in number density still achieved spectral results of the same order of magnitude as the actual FLR spectrum.

[30] The event on 21 February 1993 was found to have magnetic FLRs and pulsating arcs (630.0 nm) with frequencies close to 2.6 mHz. Another event on 31 January 1997 found FLRs and pulsating arcs at ~1.4 mHz. For both case studies the FLRs have frequencies an order of magnitude lower than the expected FLR frequency on dipolar field lines. The technique of using stretched field line eigenmodes allowed successful comparison of the experimental and model FLR spectrum for these events. The model spectrum is very close to the actual observations and more than an order of magnitude smaller than for a dipole field. The model thus provides a validation of the technique used to fit the magnetic topology, and the successful coupling of these two models also lends credence to the postulate that stretching of the magnetic field lines is at least partially responsible for anomalously low-frequency FLRs observed in auroral zone observations.

References

Baker, D. N., and R. L. McPherron, Extreme energetic particle decreases near geostationary orbit: A manifestation of current diversion within the inner plasma sheet, *J. Geophys. Res.*, *95*, 6591, 1990.

Baker, D. N., T. I. Pulkkinen, R. L. McPherron, J. D. Craven, L. A. Frank, R. D. Elphinstone, J. S. Murphree, J. F. Fennell, R.E. Lopez, and T. Nagai, CDAW-9 analysis of magnetospheric events on May 3, 1996: Event C, *J. Geophys. Res.*, *98*, 3815, 1993.

Baker, K. B., and S. Wing, A new magnetic coordinate system for conjugate studies at high latitudes, *J. Geophys. Res.*, *94*, 9139, 1989.

Baumjohann, W., G. Paschmann, and C. A. Cattell, Average plasma properties in the central plasma sheet, *J. Geophys. Res.*, *94*, 6597, 1989.

Bhattacharjee, A., C. A. Kletzing, Z. W. Ma, N. F. Otani, and X. Wang, Four-field model for dispersive field line resonances: Effects of coupling between shear-Alfén and slow modes, *Geophys. Res. Lett.*, *26*, 3281, 1999.

Borovsky, J. E., M. F. Thompson, and R. C. Elphic, The driving of the plasma sheet by the solar wind, *J. Geophys. Res.*, *103*, 17,617, 1998.

Büchner, J., and L. M. Zelenyi, Chaotization of the electron motion as the cause of an internal magnetotail instability and the substorm onset, *J. Geophys. Res.*, *92*, 13,456, 1987.

Canny, J., A computational approach to edge detection, *IEEE Trans. Pattern Anal. Mach. Intel., PAMI-8*, 679, 1986.

Daniell, R. E., Jr., and D. J. Strickland, Dependence of auroral middle UV emissions on the incident electron spectrum and neutral atmosphere, *J. Geophys. Res.*, *91*, 321, 1986.

Delcourt, D. C., J.-A. Sauvaud, R. F. Martin, and T. E. Moore, On the nonadiabatic precipitation of ions from the near-Earth plasma sheet, *J. Geophys. Res.*, *101*, 17,409, 1996.

Fairfield, D. H., An evaluation of the Tsyganenko magnetic field model, *J. Geophys. Res.*, *96*, 1481, 1991.

Fenrich, F. R., J. C. Samson, G. Sofko, and R. A. Greenwald, ULF high and low-m field line resonances observed with SuperDARN, *J. Geophys. Res.*, *100*, 21,535, 1995.

Friedrich, E., J. C. Samson, I. Voronkov, and G. Rostoker, Dynamics of the substorm expansive phase, *J. Geophys. Res.*, *106*, 13,145, 2001.

Harris, E. G., On a plasma sheath separating regions of oppositely directed magnetic field, *Nuovo Cimento*, *23*, 115, 1962.

Huang, C. Y., and L. A. Frank, A statistical study of the central plasma sheet, *Geophys. Res. Lett.*, *13*, 652, 1986.

Iijima, T., et al., Substorm currents in the equatorial magnetotail, *J. Geophys. Res.*, *98*, 17,283, 1993.

Kaufmann, R. L., Substorm currents: Growth phase and onset, *J. Geophys. Res.*, *92*, 7471, 1987.

Kubyshkina, M. V., V. A. Sergeev, and T. I. Pulkkinen, Hybrid input algorithm: An even-oriented magnetospheric model, *J. Geophys. Res.*, *104*, 24,977, 1999.

Lennartsson, W., A scenario for solar wind penetration of Earth's magnetic tail based on ion composition data from the ISEE 1 spacecraft, *J. Geophys. Res.*, *97*, 19,221, 1992.

Lennartsson, W., and E. G. Shelley, Survey of 0.1–16 keV/e plasma sheet ion composition, *J. Geophys. Res.*, *91*, 3061, 1986.

Liu, W. W., G. Rostoker, and J. C. Samson, Precipitation of hot protons from a stretched near-Earth current sheet, *COSPAR Colloq. Ser.*, *9*, 165, 1998.

Lotko, W. A., V. Streltsov, and C. W. Carlson, Discrete auroral arc, electrostatic shock and suprathermal electrons powered by dispersive, anomalously resistive field line resonanace, *Geophys. Res. Lett.*, *25*, 4449, 1998.

Lu, G., N. A. Tsyganenko, A. T. Y. Lui, H. J. Singer, T. Nagai, and S. Kokubun, Modeling of time-evolving magnetic fields during substorms, *J. Geophys. Res.*, *104*, 12,327, 1999.

Lund, E. J., E. Möbius, R. E. Ergun, and C. W. Carlson, Mass-dependent effects in ion conic production: The role of parallel electric fields, *Geophys. Res. Lett.*, *26*, 3593, 1999.

Lyons, L. R., and T. W. Speiser, Evidence for current sheet acceleration in the geomagnetic tail, *J. Geophys. Res.*, *87*, 2276, 1982.

Nakai, H., Y. Kamide, and C. T. Russell, Influences of solar wind parameters and geomagnetic activity on the tail lobe magnetic field: A statistical study, *J. Geophys. Res.*, *96*, 5511, 1991.

Nakai, H., Y. Kamide, and C. T. Russell, Statistical nature of the magnetotail current in the near-Earth region, *J. Geophys. Res.*, *102*, 9573, 1997.

Newell, P. T., V. A. Sergeev, G. R. Bikkuzina, and S. Wing, Characterizing the state of the magnetosphere: Testing the ion precipitation maxima latitude (b2i) and the ion isotropy boundary, *J. Geophys. Res.*, *103*, 4739, 1998.

Pulkkinen, T. I., et al., Modeling the growth phase of a substorm using the Tsyganenko model and multi-spacecraft observations: CDAW-9, *Geophys. Res. Lett.*, *18*, 1963, 1991.

Pulkkinen, T. I., D. N. Baker, R. J. Pellinen, J. Büchner, H. E. J. Koskinen, R. E. Lopez, R. L. Dyson, and L. A. Frank, Particle scattering and current sheet stability in the geomagnetic tail during the substorm growth phase, *J. Geophys. Res.*, *97*, 19,283, 1992.

Pulkkinen, T. I., D. N. Baker, L. L. Cogger, T. Mukai, and H. J. Singer, Coupling of inner tail and midtail processes, in *Substorms-4*, edited by S. Kokubun and Y. Kamide, p. 749, Terra Sci., Tokyo, 1998.

Pulkkinen, T. I., D. N. Baker, L. L. Cogger, L. A. Frank, J. B. Sigwarth, S. Kokubun, T. Mukai, H. J. Singer, J. A. Slavin, and L. Zelenyi, Spatial extent and dynamics of a thin current sheet during the substorm growth phase on December 10, 1996, *J. Geophys. Res.*, *104*, 28,475, 1999.

Rankin, R., J. C. Samson, and V. T. Tikhonchuk, Discrete auroral arcs and nonlinear dispersive field line resonances, *Geophys. Res. Lett.*, *26*, 663, 1999.

Rankin, R., F. Fenrich, and V. T. Tikhonchuk, Shear Alfvén waves on stretched magnetic field lines near midnight in Earth's magnetosphere, *Geophys. Res. Lett.*, *27*, 3265, 2000.

Rostoker, G., et al., CANOPUS—A ground-based instrument array for remote sensing the high latitude ionosphere during the ISTP/GGS program, *Space Sci. Rev.*, *71*, 743, 1995.

Ruohoniemi, J. M., R. A. Greenwald, K. B. Baker, and J. C. Samson, HF radar observations of Pc5 field line resonances in the midnight/early morning MLT sector, *J. Geophys. Res.*, *96*, 15,697, 1991.

Samson, J. C., Mapping substorm intensifications from the ionosphere to the magnetosphere, in *Proceedings of the International Conference on Substorms 2*, edited by J. R. Kan, J. D. Craven, and S.-I. Akasofu, p. 189, Univ. of Alaska, Fairbanks, 1994.

Samson, J. C., T. J. Hughes, F. Creutzberg, D. D. Wallis, R. A. Greenwald, and J. M. Ruohoniemi, Observations of a detached discrete arc in association with field line resonances, *J. Geophys. Res.*, *96*, 15,683, 1991.

Samson, J. C., L. R. Lyons, P. T. Newell, F. Creutzberg, and B. Xu, Proton aurora and substorm intensifications, *Geophys. Res. Lett.*, *19*, 2167, 1992.

Samson, J. C., L. L. Cogger, and Q. Pao, Observations of field line resonances, auroral arcs, and auroral vortex structure, *J. Geophys. Res.*, *101*, 17,373, 1996.

Sergeev, V. A., and M. V. Malkov, Diagnostics of the magnetic configuration of the plasma layer from measurements of energetic electrons above the ionosphere, *Geomagn. Aeron.*, *28*, 549, 1988.

Sergeev, V. A., P. Tanskanen, K. Mursula, A. Korth, and R. C. Elphic, Current sheet thickness in the near Earth plasma sheet during substorm growth phase, *J. Geophys. Res.*, *95*, 3819, 1990.

Sergeev, V. A., M. Malkov, and K. Mursula, Testing the isotropic boundary algorithm method to evaluate the magnetic field configuration in the tail, *J. Geophys. Res.*, *98*, 7609, 1993a.

Sergeev, V. A., D. G. Mitchell, C. T. Russell, and D. J. Williams, Structure of the tail plasma/current sheet at 11 R_E and its changes in the course of a substorm, *J. Geophys. Res.*, *98*, 17,345, 1993b.

Sergeev, V. A., T. I. Pulkkinen, R. J. Pellinen, and N. A. Tsyganenko, Hybrid state of the tail magnetic configuration during steady convection events, *J. Geophys. Res.*, *99*, 23,571, 1994.

Singer, H. J., D. J. Southwood, R. J. Walker, and M. G. Kivelson, Alfvén wave resonances in a realistic magnetospheric magnetic field geometry, *J. Geophys. Res.*, *86*, 4589, 1981.

Slavin, J. A., et al., An ISEE 3 study of average and substorms conditions in the distant magnetotail, *J. Geophys. Res.*, *90*, 10,875, 1985.

Streltsov, A., and W. Lotko, Small-scale "electrostatic" auroral structures and Alfvén waves, *J. Geophys. Res.*, *104*, 4411, 1999.

Strickland, D. J., R. R. Meier, J. H. Hecht, and A. B. Christensen, Deducing composition and incident electron spectra from ground-based auroral optical measurements: Theory and model results, *J. Geophys. Res., 94*, 13, 527, 1989.

Tikonchuk, V. T., and R. Rankin, Electron kinetic effects in standing shear Alfvén waves in the dipolar magnetosphere, *Phys. Plasmas*, *7*, 2630, 2000.

Tröndsen, T. S., L. L. Cogger, and J. C. Samson, Asymmetric multiple auroral arcs and inertial Alfvén waves, *Geophys. Res. Lett.*, *24*, 2945, 1997.

Tsyganenko, N. A., Global quantitative models of the geomagnetic field in the cislunar magnetosphere for different disturbance levels, *Planet. Space Sci.*, *35*, 1347, 1987.

Tsyganenko, N. A., A magnetospheric magnetic field model with a warped tail current sheet, *Planet. Space Sci.*, *37*, 5, 1989.

Tsyganenko, N. A., Modeling the Earths magnetospheric magnetic field confined within a realistic magnetopause, *J. Geophys. Res.*, *100*, 5599, 1995.

Tsyganenko, N.A., Effects of the solar wind conditions on the global magnetospheric configuration as deduced from data-based models, in *Proceedings of ICS-3 Conference on Substorms*, Eur. Space Agency Spec. Publ., ESA SP-389, 181, 1996.

Walker, A. D. M., J. M. Ruohoniemi, K. B. Baker, R. A. Greenwald, and J. C. Samson, Spatial and temporal behavior of ULF pulsations observed by the Goose Bay HF radar, *J. Geophys. Res.*, *97*, 12,187, 1992.

Wanliss, J. A., J. C. Samson, On the use of photometer data to map dynamics of the magnetotail current sheet during substorm growth phase, *J. Geophys. Res.*, *105*, 27,673, 2000.

Waters, C. L., J. C. Samson, and E. F. Donovan, Variation of plasma trough density derived from magnetospheric field line resonances, *J. Geophys. Res.*, *101*, 24,737, 1996.

West, H. I., R. M. Buck, and M. G. Kivelson, On the configuration of the magnetotail near midnight during quiet and weakly disturbed periods: Magnetic field modeling, *J. Geophys. Res.*, *83*, 3819, 1978.

Zelenyi, L., A. Galeev, and C. F. Kennel, Ion precipitation from the inner plasma sheet due to stochastic diffusion, *J. Geophys. Res.*, *95*, 3871, 1990.

Zwingmann, W., Self-consistent magnetotail theory: Equilibrium structures including arbitrary variation along the tail axis, *J. Geophys. Res.*, *88*, 9101, 1983.

———————————

R. Rankin, J. C. Samson, and J. A. Wanliss, Department of Physics, University of Alberta, Edmonton, Alberta, Canada T6G 2J1. (rankin@ space.ualberta.ca; samson@space.ualberta.ca; wanliss@space.ualberta.ca)

V. T. Tikhonchuk, Institut de Physique Fondamentale, Universite Bordeaux 1, Le Haut Vigneau, B.P. 120, F-33175 Gradignan Cedex, France.